Engineering Structures 124 (2016) 418–428

Contents lists available at ScienceDirect

Engineering Structures

journal homepage: www.elsevier.com/locate/engstruct

Effect of arrangement of tensile reinforcement on flexural stiffness and cracking

Viktor Gribniak [a,b,*], Alejandro Pérez Caldentey [c,d], Gintaris Kaklauskas [a,b], Arvydas Rimkus [a,b], Aleksandr Sokolov [a,b]

[a] Research Laboratory of Innovative Building Structures, Vilnius Gediminas Technical University, Vilnius, Lithuania
[b] Department of Bridges and Special Structures, Vilnius Gediminas Technical University, Vilnius, Lithuania
[c] Polytechnic University of Madrid, Madrid, Spain
[d] FHECOR Consulting Engineers, Madrid, Spain

ARTICLE INFO

Article history:
Received 16 April 2015
Revised 19 April 2016
Accepted 20 June 2016
Available online 6 July 2016

Keywords:
Reinforced concrete
Experiments
Deformations
Tension stiffening
Cracking

ABSTRACT

Due to the highly complex cracking behaviour of reinforced concrete structures, their design for serviceability is one of the most challenging tasks of engineering practice. Existing test data support a general inference that the deformation behaviour of concrete elements is affected by the arrangement of reinforcement in the tensile zone. Most of the current design approaches are based on the experimental data of laboratory specimens with simplified arrangement of the reinforcement. Consequently, the corresponding models are often inadequate to predict deformations and cracking of elements with non-conventional distribution of the bars. In the current study, the number of the reinforcement layers is found to correlate with the flexural stiffness. The paper also compares the crack width and crack spacing experimentally determined in the beams with different numbers of reinforcement layers. The results to some extent seem to be in conflict with the generally accepted concept relating crack widths to the cracking distances. Although the observed crack distances of the beams with three layers of bars were larger, their maximum crack openings were smaller than in the conventionally reinforced specimens with the same reinforcement ratio.

1. Introduction

One of the causes of deterioration of reinforced concrete structures is excessive cracking resulting from either restrained deformation or external loads. Reinforcing layout is designed for resisting tensile stresses in particular regions of concrete structures. A proper arrangement of reinforcement offers an alternative to increase the flexural stiffness and alleviate the cracking problems [1]. Following current design regulations of spacing and dimensioning of bars, it is common to distribute tensile reinforcement in several layers [2]. The consequent increase of number of reinforcement layers may improve deformation properties and cracking resistance of concrete members [3,4]. In order to optimize reinforcement schemes and to design cost effective structures, the effect of the arrangement of reinforcement bars in the tension zone on serviceability properties (deformations and cracking) requires an assessment and consideration for design.

Most of the current design approaches are based on experimental data of laboratory specimens with simplified arrangement of reinforcement and conventional width of the concrete cover [5,6]. Consequently, the corresponding predictions are in good agreement with the experimental results of conventionally reinforced elements [7,8], but these models are often inadequate to predict the cracking behaviour of elements with non-conventional arrangement of the bars [9–11].

Existing test data support a general inference that the flexural behaviour of concrete beams is affected by the arrangement of reinforcement bars in the tensile zone [9,12]. In cracking problems, this effect is often related to the effective area issue [6,13,14]. In deformation analysis, the increase in flexural stiffness can be accounted for by modification of the effective depth [15,16]. In the present study, the latter possibility is illustrated by fitting predictions by Model Code 2010 [17] to achieve best agreement between the theoretical and the experimental moment-curvature relationships. The paper also deals with the effect of distribution of the tensile reinforcement on the flexural cracking. It compares the crack width and crack spacing experimentally determined in the beams with different numbers of reinforcement layers. To

* Corresponding author at: Department of Bridges and Special Structures, Vilnius Gediminas Technical University, Sauletiekio av. 11, Vilnius LT-10223, Lithuania.
E-mail address: Viktor.Gribniak@vgtu.lt (V. Gribniak).

http://dx.doi.org/10.1016/j.engstruct.2016.06.026
0141-0296/

assess the crack distance, the authors propose a numerical procedure for analysis of digital images.

2. Experimental investigation on deformations and cracking of RC beams

Test specimens with different arrangements of reinforcement in the tension zone are considered. The experimental program includes bending tests of nine beams reinforced with glass fibre reinforced polymer (GFRP) or steel bars. Surface shapes of the reinforcement bars are presented in Fig. 1. For the purpose of comparative analysis, all the test specimens had identical concrete cross-sections with a similar concrete strength f_{cm} and two different reinforcement ratios p (0.6 and 1.0%).

2.1. Description of test specimens

The main parameters of the beams are listed in Table 1 with sectional notations evident from Fig. 2. Other parameters presented in the table are the concrete $\varnothing 150 \times 300$ mm cylinder compressive strength ($f_{cm,28}$) and (f_{cm}) at 28 day and at age of testing (t); the elastic modulus of steel (E_s) and GFRP (E_f); the ultimate GFRP strength (f_u) and steel yielding strength (f_y) of the reinforcement bars. Tensile strength and elasticity modulus of concrete (required for theoretical assessment of the serviceability parameters by the Model Code 2010 [17]) were calculated using the material properties from Table 1.

The presented data is part of large experimental program [18]. The beams were made using the same concrete grade (C 37) from different local producers. This investigation considers two concrete mixes given in Table 2 and denoted as *Mix A* and *Mix B*. As a part of the test program supported by the *Research Council of Lithuania*, this study employs original notations of the specimens. Letter "*S*" refers to the type of elements (in Lithuanian "Sija" = "Beam"); the first number corresponds to the level of reinforcement ratio p ("*2*" refers to $p \approx 0.6\%$ and "1" to $p \approx 1.0\%$); "*nm*" refers to non-metallic (GFRP) reinforcement. The experimental beams were cast using steel formworks. The beams were unmolded in 2–3 days after casting. The specimens were cured at an average relative humidity (*RH*) of 73% and a temperature of 20 °C.

2.2. Testing procedure

The experimental beams with a nominal length of 3280 mm were tested under a four-point bending scheme with 1000 mm shear spans as shown in Fig. 3 that also gives the strain gauge position. The specimens were loaded with a 1000 kN hydraulic jack in a stiff testing frame. The test was performed with small increments (2 kN) and paused for short periods (about 2 min) to take readings of the gauges and to measure crack development. On average, it took 50–80 load increments with a total test duration of 3 h. The testing equipment acting on the beam weighed 2.3 kN. The latter summed up with the beam's own weight induced a 3.5 kN m bending moment at mid-span.

Moment-curvature diagrams were obtained in two ways: from deflections and from concrete surface strains, both recorded in the pure bending zone. Concrete surface strains were measured throughout the length of the pure bending zone, using mechanical 200 mm gauges. As shown in Fig. 3 (view 'A'), four continuous gauge lines (with five gauges in each line) were located at different heights. The two extreme gauge lines were placed along the top and the bottom reinforcement whereas two other lines were located 60 mm off these lines. To measure deflections, linear variable differential transducers (L_1–L_8, see Fig. 3) were placed beneath the soffit of each of the beams. Previous studies [19–22] revealed good agreement between the moment-curvature diagrams obtained from the deflection of the pure bending zone and strain measurements. In the present study, the moment-curvature response of the beams was assessed using the strains averaged along each of the gauge lines shown in Fig. 3. Following the methodology detailed in Refs. [19,20], the curvature averaged through the pure bending zone is calculated as:

$$\kappa = \frac{1}{6}\sum_{l=2}^{4}\sum_{k=1}^{l-1}\frac{D_k - D_l}{h_{kl}}. \quad (1)$$

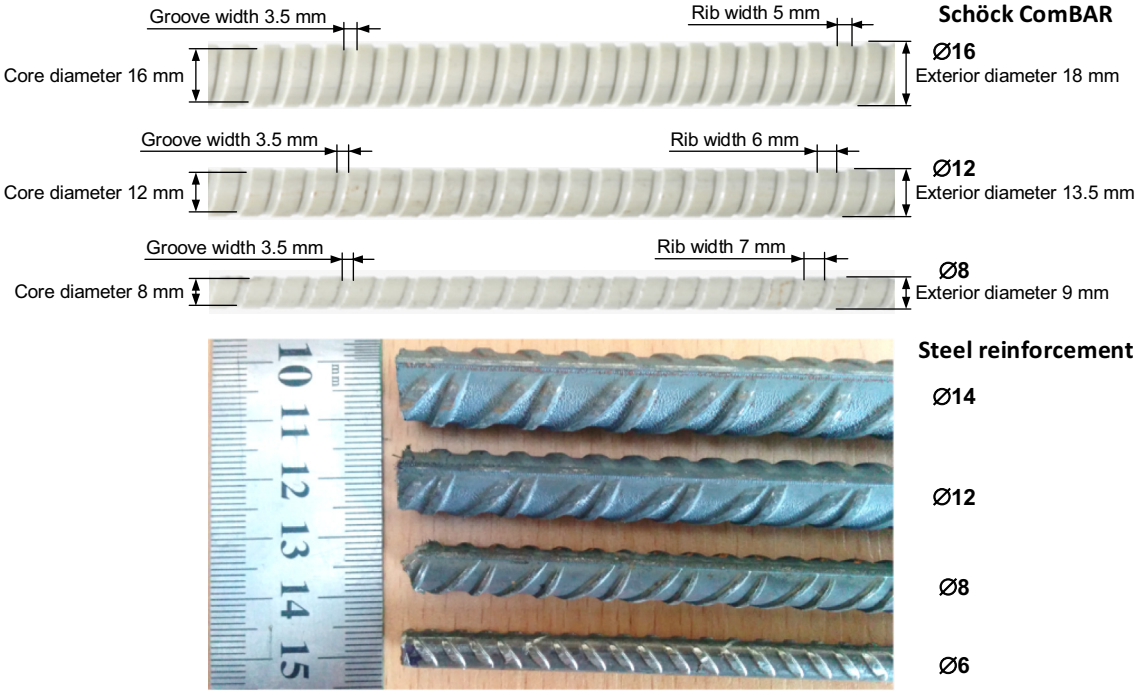

Fig. 1. Reinforcement bars.

Table 1
Main characteristics of the test beam.

Beam	h	d[a]	a_2	b	A_1	A_2	np	$f_{cm,28}$	f_{cm}	t	E_s	E_f	f_y	f_u	Mix
	mm				mm^2		%	MPa		days	GPa		MPa		
S1-1	299	248	25	282	695.9	56.6	5.70	45.52	49.7	75	209.9	–	578.1	–	*B*
S1-6	303	217	37	271	603.2	56.6	5.76	39.55	43.0	256	209.8	–	589.0	–	*A*
S2-1	301	254	30	279	429.9	56.6	3.60	45.52	49.4	73	223.5	–	585.4	–	*B*
S2-5nm	302	246	26	276	452.4	56.6	1.12	41.29	56.0	167	–	65.1	–	1491	*A*
S1-2	300	273	29	284	776.8	56.6	5.62	45.52	49.4	67	210.5	–	632.3	–	*B*
S1-4	300	267	24	280	760.0	56.6	5.47	45.52	49.4	68	199.3	–	551.1	–	*B*
S1-5-2nm	305	275	33	277	804.2	56.6	1.89	38.37	44.6	236	–	65.1	–	1491	*A*
S2-3	300	272	29	282	466.1	56.6	3.44	42.51	48.1	66	210.5	–	632.3	–	*B*
S2-4-2nm	303	272	27	276	452.4	56.6	1.06	47.21	49.4	37	–	64.7	–	1468	*A*

[a] The effective depth is given with respect to the centroid of tensile reinforcement.

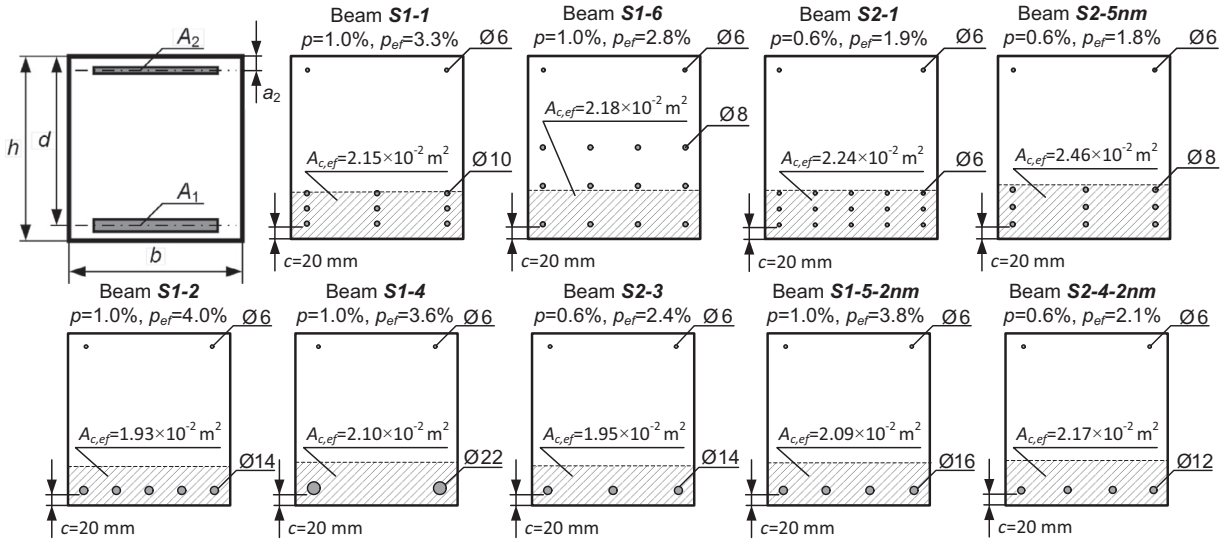

Fig. 2. Cross-sections of the test beams with different distribution of reinforcement bars in the tensile zone.

Table 2
Mix proportions [kg/m^3].

Material	*Mix A*	*Mix B*
Sand 0/4 mm	910 ± 2%	905 ± 2%
Crushed aggregate 5/8 mm	940 ± 2%	388 ± 1%
Crushed aggregate 11/16 mm		548 ± 1%
Cement CEM I 42.5 N	415 ± 1%	400 ± 0.5%
Water	174 ± 5%	124 ± 5%
Concrete plasticizer *Stachement 2067*	3.32 ± 2%	–
Concrete plasticizer *Muraplast FK 63.30*	–	2 ± 2%

Here D_k and D_l are the averaged strains along k and l gauge lines (1st…4th lines, Fig. 3), respectively; h_{kl} is the distance between the lines (k, $l = 1…4$, $k \neq l$). Fig. 4 shows the obtained moment-curvature diagrams.

The crack pattern was marked during the tests at the side of the beams, opposite to that where surface deformation measurements were taken (Fig. 3). At the chosen loading levels, the crack width was measured at the gravity centre of the tensile reinforcement using a 50 magnification (50×) optical microscope. Additionally, development of the visible cracks was located specifying the crack shape under the particular loading level. Fig. 5 represents the final crack pattern of the beams, indicating the load levels for which the cracks reach a given web depth, thereby obtaining a representation of the crack development with load.

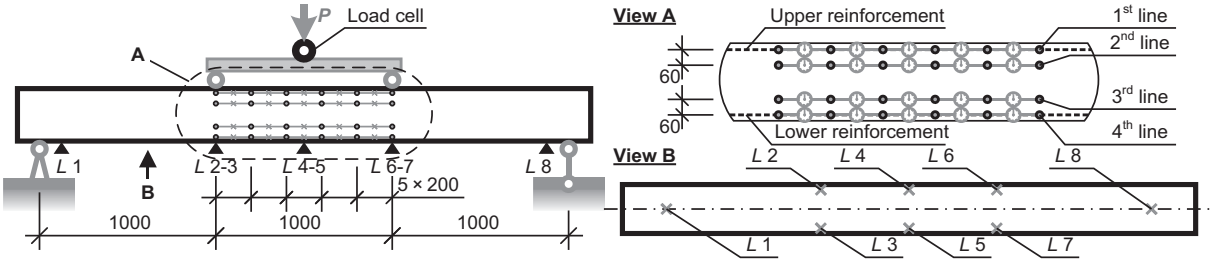

Fig. 3. Loading system and arrangement of test devices.

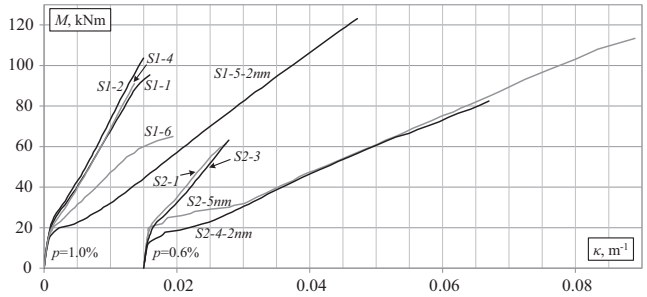

Fig. 4. Moment-curvature response of the beams.

3. Deformation analysis

3.1. Accuracy analysis

In Fig. 6, Model Code 2010 (MC 2010) [17] predictions are compared with the experimental moment-curvature diagrams. Two types of behaviour can be observed comparing the experimental and predicted diagrams: with increasing load, beams with one layer of reinforcement exhibit a progressive degradation of the stiffness, with respect to values predicted by MC 2010, whereas the actual stiffness of the beams with multiple layers of the bars does not exhibit such a degradation until failure. The differences in deformation behaviour of the beams can be explained by variations in effective depth (taken in specimens with three layers of bars as the distance from the middle layer to the top concrete surface) and the arrangement of tensile bars, as these were the only differences between the beams. As can be observed in Fig. 2, all beams had a constant nominal cover ($c = 20$ mm), which did not secure sufficient confinement causing initiation of splitting cracks and, consequently, degradation of overall stiffness. On the contrary, a large number of bars closely distributed in the tensile zone safeguarded high relative stiffness of the cracked specimen throughout all loading stages. Similar results were obtained in the tests of tensile members [3,4,23,24], and beams [10,20,25,26], reinforced with a large number of closely spaced bars. Such members have demonstrated significant increase of stiffness of the cracked section (with respect to the specimens with conventional distribution of reinforcement in the tension zone).

In the current study, to assess differences in the stiffness, the curvature predictions by the MC 2010 were used as reference.

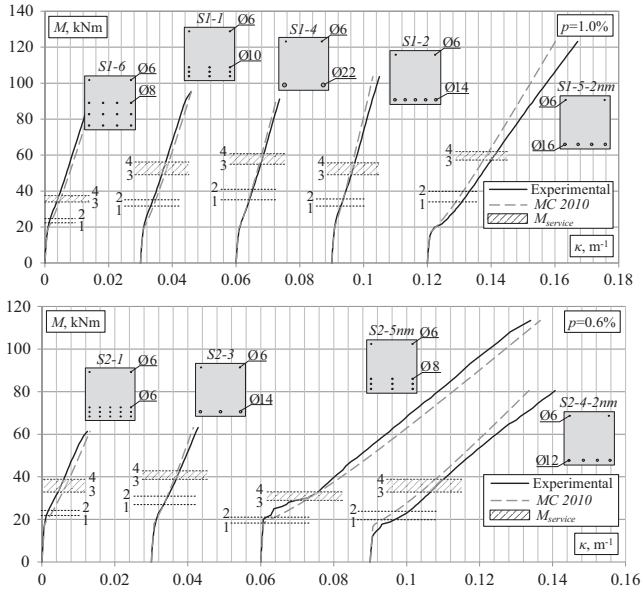

Fig. 6. Comparison of experimental and predicted moment-curvature behaviour.

The curvature results in different specimens were compared using the relative term:

$$\Delta\kappa = \frac{\kappa_{obs} - \kappa_{MC}}{\kappa_{obs}}. \quad (2)$$

Here κ_{obs} and κ_{MC} are the observed and calculated (reference) curvatures, respectively.

For comparative analysis purposes, the deformational behaviour of the test specimens was investigated at four *reference* levels of loading intensity related to the reference ultimate bending moment M_u. This value was *calculated* assuming the strength limit of 500 MPa for the bar reinforcement. Table 3 shows the characteristic load levels and the corresponding values of the relative curvature, $\Delta\kappa$, from Eq. (2). Additionally to the reference load levels, the predictions at the *service* load, M_{ser}, were analysed. This loading level is of vital importance in the design for serviceability [10,27]. As can be observed from Table 3 and Fig. 6, the service load is within the bounds described by "**3**" and "**4**" reference points.

In Table 3, the beams are presented in two groups – the first four specimens with three layers of the tensile bars included in

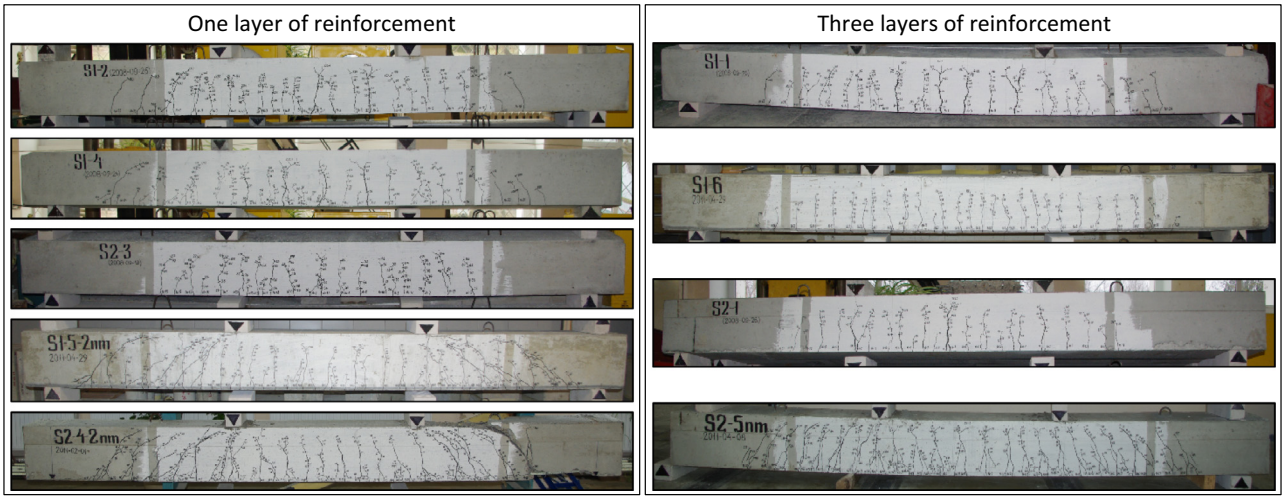

Fig. 5. Final crack pattern.

Table 3
Relative curvature prediction percentage, $\Delta\kappa$, determined at the loading levels highlighted in Fig. 6.

Group	Beam	M_u, kN m	Loading level				
			1 (0.32–0.33 · M_u)	**2** (0.36–0.39 · M_u)	**3** (0.48–0.54 · M_u)	**4** (0.58–0.63 · M_u)	M_{ser} (0.55 · M_u)
I	*S1-1*	92.24	−36.3	−23.7	−14.2	−13.0	−13.6
	S1-6	59.95	−92.9	−71.9	−34.6	−30.2	−32.2
	S2-1	60.56	−62.3	−84.6	−35.3	−25.8	−29.7
	S2-5nm	52.74	−15.2	−85.9	−49.2	−4.7	−20.7
II	*S1-2*	122.89	3.0	8.6	10.4	11.1	10.8
	S1-4	103.52	3.7	4.6	6.4	6.9	6.7
	S1-5-2nm	101.48	18.6	16.7	12.3	12.2	12.2
	S2-3	75.71	−2.1	1.4	7.6	7.9	7.8
	S2-4-2nm	58.77	57.1	41.5	18.3	11.9	14.9

Group I. Whereas, Group II represents the specimens with the reinforcement distributed in one layer (Fig. 6). It is evident that the deformation behaviour of the beams from these two groups are different. The authors' viewpoint is that a prediction is safe, if $\Delta\kappa \leqslant 0$, since the physical nature of the ratio $\Delta\kappa$ means that the code overestimates the deflection in such cases. MC 2010 overestimated deformations (curvatures) of the elements from the first group at all considered loading levels: at the service load, the overestimation of the predictions (the prediction safety) varies from 14% to 32%. On the contrary, deformations of the beams with conventional distribution of the reinforcement (in one layer with minimal cover) were underestimated almost at all loading stages: at the service loading, deficiency of the predictions was found equal to 7–15%. The obvious differences of the predictions between the groups inspire a modification of the deflection prediction for the specimens with three layers of the reinforcement.

3.2. Modifying the effective depth

Previous research by the authors [10,20,26] has shown that tension stiffening might increase noticeably in the beams with three (or more) layers of closely distributed reinforcement bars. As mentioned in the introduction, the increase in flexural stiffness can be taken into account by modifying the effective depth, d [16]. For the purposes of illustration of the dependency of d on the variation of the effective reinforcement ratio, the effective depth was fitted to achieve best agreement between the theoretical and the experimental moment-curvature relationships. For the considered beams with three layers of reinforcement, the modified depth can be obtained from the following equation:

$$d_{mod} = d \cdot \left(1.13 - 0.078\frac{p_{ef}}{n}\right). \tag{3}$$

Here d is the effective depth; p_{ef} is the effective reinforcement percentage; n is the modular ratio E_s/E_c. The modified moment-curvature diagrams are shown in Fig. 7 with the relative predictions $\Delta\kappa$ [from Eq. (2)] presented in Table 4. As can be observed from Tables 3 and 4, this modification improves predictions securing a rational safety margins for the service loads, M_{ser}.

To analyse the variation of the prediction errors with load, Fig. 8 scatters the predictions $\Delta\kappa$ along the normalized loading level M' determined as

$$M' = \frac{M - M_{cr}}{M_u - M_{cr}}. \tag{4}$$

Here M_u is the theoretical ultimate bending moment (assuming reinforcement strength 500 MPa); M_{cr} is the theoretical cracking moment. According to Eq. (4), $M' = 0$ and $M' = 1$ correspond to the cracking and ultimate moments, respectively.

Along the predictions $\Delta\kappa$, Fig. 8 shows the corresponding trends determined by the means of moving average (with period of 10 points). It can be observed that very accurate prediction results were obtained at the advanced loading stages with M' ranging from 0.5 to 1.0. However, at the earlier cracking stages ($0.1 < M' < 0.5$), the predicted curvatures remained significantly overestimated. In other words, the considered beams resisted development of the cracks quite efficiently until the relative load M' reached 0.5. However, it should be recalled that the present analysis is limited to the test results (202 curvature points) of only *four* beams with different layouts of the tensile reinforcement; therefore, a more elaborate experimental study is needed to further quantify the empirical relationship (3).

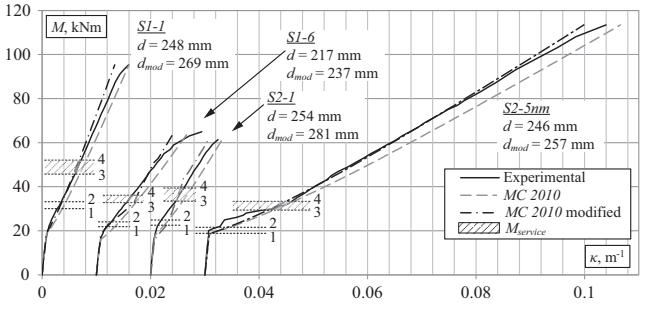

Fig. 7. The improved moment-curvature prediction results.

Table 4
Modified curvature prediction percentage, $\Delta\kappa$, determined at the loading levels highlighted in Fig. 6.

Beam	Loading level				
	1 (0.32–0.33 · M_u)	**2** (0.36–0.39 · M_u)	**3** (0.48–0.54 · M_u)	**4** (0.58–0.63 · M_u)	M_{ser} (0.55 · M_u)
S1-1	−13.9	−3.3	4.6	5.6	5.1
S1-6	1.9	4.1	−24.1	−19.4	−21.5
S2-1	−111.9	−119.4	−12.0	6.4	−1.2
S2-5nm	−15.0	−75.1	−36.3	4.4	−10.3

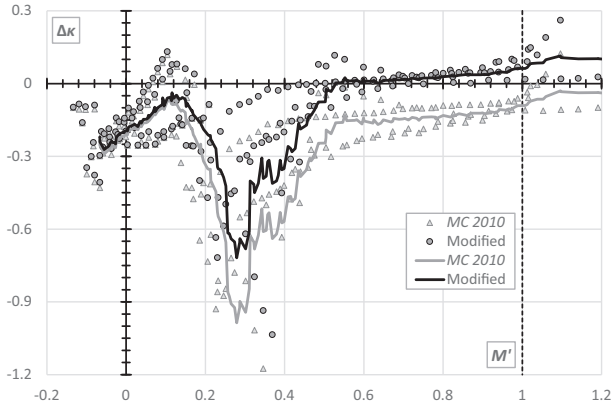

Fig. 8. Relative curvature predictions, $\Delta\kappa$, of the beams with multiple number of reinforcement layers.

4. Cracking analysis

4.1. Distance between the cracks

The distance between cracks is the governing parameter for the crack width prediction. However, assessment of crack distances in some cases is not so straightforward. At different loading stages, cracks appear with different spacing, length, and width. Therefore, frequently estimation of the cracking parameters might be very subjective. To avoid subjectivity of the judgement, a numerical procedure for determination of the distances between cracks has been developed. The location of a crack is defined as the centroid of the projection of the crack on the longitudinal axis of the specimen. The current analysis considers the cracking behaviour in the pure bending zone. Fig. 9 sketches the procedure for obtaining the crack distances that consists of following steps:

(1) At a given loading level, the crack distribution scheme is made using the crack patterns (Fig. 5).
(2) Using horizontal lines spaced at a distance of 5 mm, the schematic cracks are "trimmed" generating an array of the cross-points.
(3) The origin of the longitudinal axis x is associated with the boundary of the pure bending zone. The collection of the projections of the generated array of the cross-points to the x-axis produces the target dataset for further clustering.

The agglomerative hierarchical clustering technique was chosen for identifying the cracking points (projections) that closely resemble one another. The clusters, related with location of the discrete cracks, were formed using the linkage function described as a shortest Euclidean distance between the elements. The 20 mm distance was chosen as a threshold for "cutting" the data into clusters. Application of the clustering technique to the datasets generated at the different loading levels results in the diagram that represents evolution of the crack distance with increasing load. The evolution diagrams of maximum crack distance are shown in Fig. 10 for all the beams. Similar graphs for the average crack distance are presented in Fig. 11. The delayed crack formation can be observed from both figures. This effect is more evident for the beams with relatively low amount of the reinforcement (p = 0.6%). The delayed cracking is closely related to the increment in stiffness, evidenced in Section 3.1.

In the assessment of differences in the crack distances in the beams with one and three layers of reinforcement, the predictions by MC 2010 were used as a reference. The clustered and the calculated maximum crack distances at the service load are compared in Table 5. As can be observed in Figs. 6 and 10 for all the beams, the stabilized cracking stage was achieved before the service load. In Table 5, the relative predictions Δs were calculated by Eq. (2), where, instead of the curvatures, the corresponding values of the maximum crack distances, i.e. experimental ($s_{r,obs}$) and calculated ($s_{r,MC}$) are considered. Similarly to the curvature analysis, Table 5 reveals differences in the relative predictions Δs. From this table, three important observations can be made:

(1) There is a general tendency that the predicted maximum crack distances are smaller in the beams of the first group having noticeably smaller diameters of the bars compared to the beams of the second group. Despite of different area of location of the tensile bars (Fig. 2), the differences between the effective heights, h_{ef}, are not that significant as they were established from two alternative governing conditions given in Table 5. In other words, the introduction of multiple layers of reinforcement does not significantly affect the effective reinforcement ratio. Thus, the predictions by the MC 2010 are mainly controlled by the diameter of the bars.
(2) Differences in the experimentally observed maximum distances between the beams of the two groups are less significant. In contrast to the predictions, the conventionally reinforced beams displayed smaller crack distances than

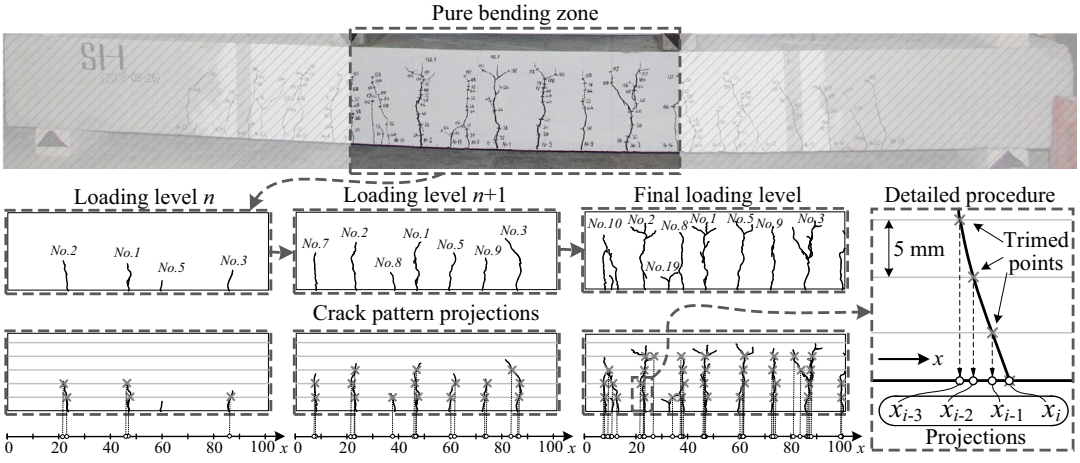

Fig. 9. Extraction of the data-points for the crack clustering procedure.

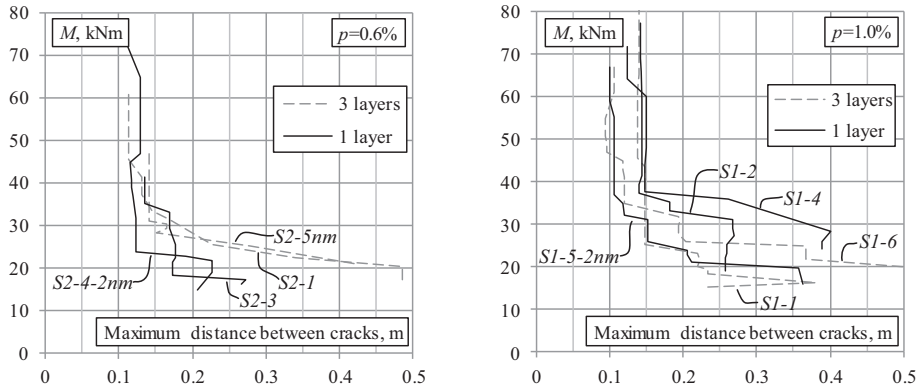

Fig. 10. Variation of maximum crack distance with load for the beams with one and three layers of reinforcement.

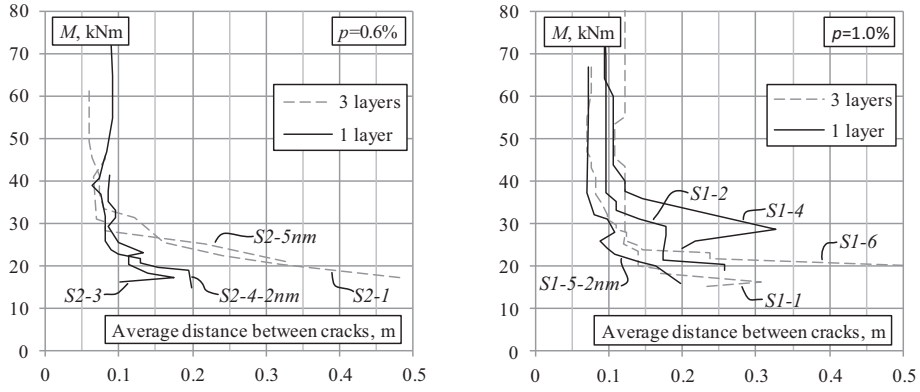

Fig. 11. Variation of mean crack distance with load for the beams with one and three layers of reinforcement.

Table 5
Experimental and calculated maximum distances between cracks, determined at the service load.

Group	Beam	Bars, (∅, mm)	Effective ratio, p_{ef} (%)	Effective height[a], h_{ef} (mm)		Crack distance, $s_{r,max}$ (mm)		Ratio, Δs (%)
				$2.5 \times (h\text{-}d)$	$(h-x)/3$	Experimental	Calculated	
I	*S1-1*	9 × ∅10	3.3	–	76.3	137.5	124.6	9.4
	S1-6	12 × ∅8	2.8	–	80.4	194.1	120.3	38.0
	S2-1	15 × ∅6	1.9	–	80.5	168.3	128.2	23.9
	S2-5nm	9 × ∅8	1.8	–	89.4	151.4	161.0	−6.3
II	*S1-2*	5 × ∅14	4.0	68.0	–	141.7	137.7	2.8
	S1-4	2 × ∅22	3.6	–	75.2	125.1	209.0	−67.1
	S1-5-2nm	4 × ∅16	3.8	75.6	–	105.7	155.7	−47.3
	S2-3	3 × ∅14	2.4	69.0	–	134.1	203.9	−52.0
	S2-4-2nm	4 × ∅12	2.1	78.5	–	122.3	199.8	−63.4

[a] The effective height is associated with the corresponding governing criteria.

the ones in the equivalent specimens with three layers of reinforcement. Providing the total area of the tensile reinforcement is constant, distribution of bars in multiple layers resulted in a delayed stabilized cracking stage (Fig. 8 evidences this effect). Consequently, the MC 2010 prediction adequacy seems to be dependent on the layout of the tensile reinforcement.

(3) The predictions for the conventionally reinforced elements noticeably overestimate the experimental values. The number of the tested specimens, however, is not sufficient to reach a reliable conclusion about the adequacy of the predictions. Further research is needed to investigate the suitability of the equations proposed by the MC 2010.

A relation between the maximum and average crack distances (Figs. 10 and 11) is another important parameter that needs clarification. The respective values of the crack distances determined using the proposed clustering procedure at "loading levels **3**" and "**4**" (Fig. 6) are given in Table 6. In Table 6, the experimental data are ranged in accordance with the ratio presented in the last column. In the considered cases, this ratio varies from 1.3 to 2.0 and is equal to 1.5 in average. This result is in agreement with the findings of other studies suggesting the ratio of maximum and mean crack spacing to be between 1.3 and 1.7 [13]. The authors also found that this ratio differed for the members with different reinforcement ratio, on average being 1.7 and 1.4, respectively for the cases of p = 0.6% and 1.0%. However, due to a limited test data and interval of the reinforcement ratio, these observations should be understood more as insights for further research than as general evidence.

It should be kept in mind that the above results were obtained based on the crack distances that were established using the

Table 6
The crack distance results for the "**3**" and "**4**" loading steps highlighted in Fig. 6.

Group	Beam	Reinforcement ratio		$\varnothing/p_{ef}$	$s_{r,max}$ (mm)		$s_{r,m}$ (mm)		$s_{r,max}/s_{r,m}$	
		p (%)	p_{ef} (%)		Step **3**	Step **4**	Step **3**	Step **4**	Step **3**	Step **4**
I	*S1-1*	1.01	3.28	3.05	137.5	137.5	108.7	108.7	1.26	1.26
II	*S1-4*	1.02	3.61	6.09	125.1	125.1	93.9	93.9	1.33	1.33
I	*S1-6*	1.03	2.77	2.89	192.8	120.3	98.5	89.6	1.96	1.34
II	*S1-5-2nm*	1.06	3.84	4.17	105.7	105.7	69.4	72.6	1.52	1.46
II	*S2-3*	0.60	2.37	5.90	134.1	134.1	85.0	87.0	1.58	1.54
II	*S2-4-2nm*	0.60	2.09	5.75	122.3	119.1	81.8	75.0	1.50	1.59
II	*S1-2*	0.99	3.98	3.52	141.7	142.3	95.0	86.4	1.49	1.65
I	*S2-1*	0.60	1.89	3.17	168.3	130.8	120.4	74.1	1.40	1.77
I	*S2-5nm*	0.67	1.84	4.35	151.4	142.0	81.6	69.4	1.86	2.04

Table 7
Width (μm) of five maximum, $w_{(1)\text{-}(5)}$, and average, w_m, cracks measured at the load stages shown in Fig. 6.

Loading level	Opening rank	Three layers of reinforcement				One layer of reinforcement				
		S1-1	*S1-6*	*S2-1*	*S2-5nm*	*S1-2*	*S1-4*	*S1-5-2nm*	*S2-3*	*S2-4-2nm*
1 (0.32–0.33 · M_u)	$w_{(1)}$	50	30	24	–	50	60	110	40	180
	$w_{(2)}$	40	20	14	–	40	60	100	40	140
	$w_{(3)}$	40	–	14	–	30	38	100	30	140
	$w_{(4)}$	40	–	14	–	24	34	90	30	100
	$w_{(5)}$	40	–	–	–	20	24	70	30	100
	w_m (cracks)	37 (7)	25 (2)	17 (4)	–	31 (10)	33 (11)	65 (10)	24 (9)	132 (5)
	$w_{(1)}/w_m$	1.35	1.20	1.41	–	1.61	1.82	1.69	1.67	1.36
2 (0.36–0.39 · M_u)	$w_{(1)}$	80	30	30	–	62	80	120	60	320
	$w_{(2)}$	70	30	30	–	50	60	110	60	300
	$w_{(3)}$	70	30	24	–	50	54	110	50	260
	$w_{(4)}$	60	20	14	–	40	50	90	40	240
	$w_{(5)}$	60	20	–	–	40	34	70	40	220
	w_m (cracks)	59 (7)	26 (5)	25 (4)	–	39 (11)	42 (11)	68 (12)	29 (11)	210 (8)
	$w_{(1)}/w_m$	1.36	1.15	1.20	–	1.59	1.91	1.77	2.07	1.52
3 (0.48–0.54 · M_u)	$w_{(1)}$	100	60	82	200	102	120	130	100	440
	$w_{(2)}$	94	60	80	200	80	90	120	80	440
	$w_{(3)}$	80	40	80	190	70	70	110	60	440
	$w_{(4)}$	70	40	80	150	62	70	110	60	420
	$w_{(5)}$	70	40	60	100	54	44	110	60	420
	w_{MC}[a]	*121*	*101*	*101*	*298*	*179*	*208*	*444*	*191*	*973*
	w_m (cracks)	71 (9)	39 (11)	59 (8)	136 (8)	59 (11)	61 (11)	77 (14)	42 (12)	350 (10)
	$w_{(1)}/w_m$	1.41	1.54	1.39	1.47	1.73	1.96	1.69	2.41	1.26
4 (0.58–0.63 · M_u)	$w_{(1)}$	124	60	102	240	142	140	140	120	480
	$w_{(2)}$	120	60	100	230	100	100	120	80	480
	$w_{(3)}$	120	60	100	200	100	100	120	80	460
	$w_{(4)}$	120	50	80	160	100	70	120	80	460
	$w_{(5)}$	100	50	80	140	90	60	110	80	460
	w_{MC}[a]	*154*	*131*	*144*	*419*	*223*	*264*	*558*	*248*	*1233*
	w_m (cracks)	93 (10)	43 (12)	74 (9)	142 (14)	88 (11)	71 (12)	81 (15)	52 (13)	376 (11)
	$w_{(1)}/w_m$	1.33	1.40	1.38	1.69	1.61	1.97	1.73	2.31	1.28

[a] Maximum crack predictions by the Model Code 2010 [17].

clustering technique. For sake of illustration, a simple approach was presented in this study that did not take into account the height of the cracks. Thus, the secondary cracks were not excluded, possibly giving reduced values of crack distances. Future research should include filtering technologies that will be able to suppress minor inputs of the clustered data. In practical terms, it would include accounting for the height of the cracks as well as possibly their width.

4.2. Crack width

The aforementioned stochastic nature and complex topology of cracks complicate crack width analysis. Furthermore, flexural cracking is dependent on the level of the measurements (within the height of the section) [28]. In this context, reliability of these measurements is rather low in comparison to the experimental data considered in the previous sections of this paper. Therefore, this section presents more a qualitative than a quantitative assessment of the results.

The analysis of the location of the maximum crack openings and the corresponding distances between the cracks is the topic of this section. This analysis is performed under the same characteristic loading levels used for the deformation analysis. Due to their time-consuming character, crack measurements were performed for a limited number of loading stages. Thus, the nearest crack width measurement was attributed to the characteristic stage under consideration. This analysis deals with measurements of the cracks located in the pure bending zone. At each loading stage, the five cracks with the maximum crack openings are considered. This experimental data is presented in Table 7; the respective crack patterns are shown in Fig. 12. The crack with the largest opening is assigned the first rank, referred to as "$w_{(1)}$".

It is important to note that Tables 5 and 7 indicate contrasting results: although the observed crack distances for the stabilized cracking stage ($0.5–0.6 \cdot M_u$) of the unconventionally reinforced beams are larger, their maximum crack openings are smaller than in the corresponding specimens with one layer of the bars. The maximum crack widths of the paired beams *S1-6* and *S1-4* differ more than twofold at all considered loading stages. Due to the decreased deformation modulus of GFRP reinforcement (Table 1), the paired elements *S2-5nm* and *S2-4-2nm* represent more extreme differences. Fig. 10 also supports this. Such result is a consequence of differences in the levels of crack monitoring – the measurements were associated with the gravity centres of the tensile reinforcement. However, it can be also linked with the fact that a bar controls cracking in its vicinity only with internal cracks closing as distance from the bar increases and deformation concentrating in a decreasing number of wider cracks [10,28–30].

Along with the experimental data, Table 7 presents crack width predictions obtained by the MC 2010 for the stabilized cracking stage. Although the reported crack width measurements could be analysed only qualitatively, overestimation of the predictions is quite evident. The relative predictions calculated by Eq. (2) vary between 20% and 120% with exception of the beams *S1-5-2nm* and *S2-4-2nm*. The latter specimens, reinforced with GFRP bars distributed in one layer (Fig. 2), demonstrate crack width overestimated two to four times. These results can be related to a limited predictive capability of the MC 2010 regarding unconventional reinforcement types, though previous research [31] has shown that within the loading stage characteristic to the serviceability analysis bond characteristics of the GFRP bars comparable to ribbed steel reinforcement. Furthermore, the general idea of the MC 2010 is to formulate a mathematical model (consistent with experimental evidence) that provides a reasonable reliability of the predictions of the maximum crack spacing and the maximum crack width that can potentially occur.

The obtained crack patterns shown in Fig. 12 illustrate the approximate nature of the assumption of direct relation between the maximum crack width and the maximum crack distance, fundamental for most of the cracking prediction models. The maximum crack opening is not necessarily located near the maximum uncracked blocks noted as max (this is true for 11 of 18 cracked

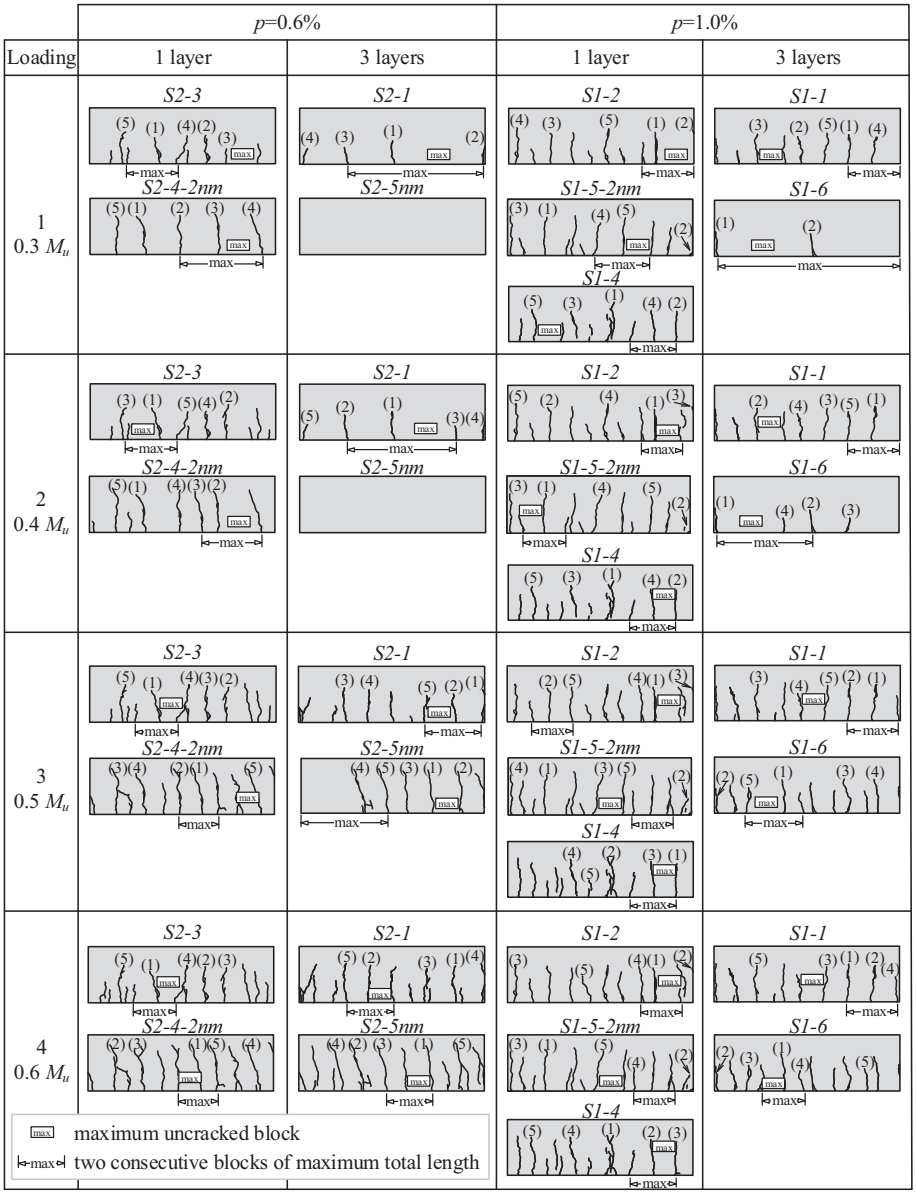

Fig. 12. Crack pattern under the reference loading levels indicated in Fig. 6 – the maximum cracks $w_{(1)}...w_{(5)}$ are designated as (1)...(5).

Table 8
Parametric analysis of the crack width results.

Group	Beam	∅ (mm)	Totalperimeter, ΣP (mm)	Reinforcement ratio, p (%)	Effective ratio, p_{ef} (%)	$\varnothing/p_{ef}$	$\varnothing/p'_{ef}$	$w_{(1)}/w_m$	
								Step **3**	Step **4**
II	*S2-4-2nm*	12	150.8	0.60	2.09	5.75	5.75	1.26	1.28
I	*S1-1*	10	282.7	1.01	3.28	3.05	3.05	1.41	1.33
I	*S2-1*	6	282.7	0.60	1.89	3.17	3.17	1.39	1.38
I	*S1-6*	8	301.6	1.03	2.77	2.89	6.33	1.54	1.40
II	*S1-2*	14	219.9	0.99	3.98	3.52	3.52	1.73	1.61
I	*S2-5nm*	8	2262	0.67	1.84	4.35	4.35	1.47	1.69
II	*S1-5-2nm*	16	201.1	1.06	3.84	4.17	4.17	1.69	1.73
II	*S1-4*	22	138.2	1.02	3.61	6.09	6.09	1.96	1.97
II	*S2-3*	14	132.0	0.60	2.37	5.90	5.90	2.41	2.31

schemes associated with the loading ranges "**3**" and "**4**"). However, in the remaining seven cases, one of the five considered maximum cracks is adjacent to the maximum length block. In this regard, it is important to note that in most cases of the latter specimens the differences between the widths of the maximum cracks (Table 7) was small.

From the theoretical point of view, in the stabilized cracking stage, the maximum crack should appear between two uncracked blocks of maximum total length (highlighted in Fig. 12). However, in the considered crack patterns, only 11 cases represent such an "ideal" crack distribution. In reality, the location of the maximum crack is related to the defects in concrete structure and/or local damages of the bond with reinforcement. The latter is important for concrete elements reinforced with a relatively small number of bars. The increase of the number of bars smears out the cracking behaviour. An elaborate discussion of this issue can be found in Ref. [10]. Comparison of the results of paired-beams (Fig. 12) reveals the fact that the number of visible cracks in the specimens with a conventional distribution of the bars is always greater than that observed in the elements with three layers of reinforcement. This observation seems to be in a conflict with the generally accepted concept relating crack widths to the cracking distances. Although the maximum crack distances observed at the stabilized cracking stage ($\approx 0.6 \cdot M_u$) were larger in the beams with the distributed reinforcement, their maximum crack openings were smaller than in the corresponding conventionally reinforced specimens. Probably, this effect might be related to the development of internal cracks around the multiple layers of the bars that are not visible on the surface.

In the analogy to the crack distances, the ratio between the maximum and average crack widths is of high importance. Thus, Table 7 includes this ratio as well as the average crack width. (The table also includes the respective number of cracks, which were averaged for.) The loading stages "**3**" and "**4**" (Fig. 6) are characteristic for the cracking analysis related with the stabilized cracking stage. In detail, this loading range is analysed in Table 8, where the experimental data are ranged in accordance to the ratio presented in the last column. From the results shown in Tables 7 and 8, the following observations can be made:

(1) The ratio between the maximum and mean crack widths, varying between 1.3 and 2.4, is equal to 1.7 in average. This ratio is about 20% larger compared to the one defined for the crack distances (Section 4.1).
(2) Unlike the crack distances, the ratio $w_{(1)}/w_m$ is dependent on the variation in the total perimeter ΣP of the reinforcement bars and the parameter $\varnothing/p_{ef}$. An exception serves beam *S2-4-2nm* that was reinforced with a single layer GFRP bars (Fig. 2). The observed discrepancy could be due to the uncertainties related to the serviceability characteristics of members with low reinforcement ratio and high deformability of the bars. This issue is discussed in more detail in Ref. [10]. If this point is discarded, it is observed that $w_{(1)}/w_m$ increases with decreasing bar perimeter and with increasing $\varnothing/p_{ef}$ ratio.

Unusual layout of the reinforcement bars in the beam *S1-6* (Fig. 2) raises the issue of adequacy of the effective reinforcement ratio. In accordance with design regulations [13], only the tensile bars being inside the effective area of the concrete are accounted for. Following this rule, only the bottom layer ($4 \times \varnothing 8$ mm bars) of the reinforcement could be taken into account resulting in the height of effective area, $h_{ef} = 58.6$ mm (compare to 80.4 mm, Table 5). Then results of the parametric analysis presented in Tables 6 and 8 assuming the reduced effective reinforcement ratio, $p'_{ef} = 1.26\%$, become less consistent as compared to the data of other specimens. The same applies to the prediction results of crack distance (Table 5) and crack width (Table 7).

5. Summary and conclusions

The study presented in this paper investigates the effect of the arrangement of tensile reinforcement on the flexural stiffness and cracking of concrete beams. The experimental data of nine beams tested by the authors have been used for this purpose. The beams were reinforced with GFRP or steel bars. Two types of the beams were considered. The first group of specimens had a conventional reinforcement layout – the bars were distributed in a single layer with minimum (20 mm) cover. The second group contains specimens with the same reinforcement ratio (as in the conventional beams), but with tensile reinforcement arranged in three layers. For the determination of measured crack distance analysis, a numerical procedure has been proposed in order to avoid subjectivity. To evaluate differences in the behaviour, the predictions by Model Code 2010 were set as the reference assuming that a prediction is safe if the code overestimates the experimental value. The study reveals that:

(1) The number of the reinforcement layers correlates with the flexural stiffness. At the service load, the deflection (curvature) predictions by the Model Code were on the safe side for the beams with three reinforcement layers (the prediction safety varied from 14% to 32%), whereas the predictions for the conventionally reinforced members were deficient by 7–15%.
(2) Although the crack spacing predictions by the Model Code for the beams with high concentration of the bars were quite accurate, the results for the conventionally reinforced elements differed significantly with the experimental values being about 50% larger than the calculated ones.

(3) The present experimental results on cracking do not reveal a clear correlation between crack widths and the crack spacing when the reinforcement layout changes. Although the observed crack distances for the stabilized cracking stage of the beams with three layers of bars were larger, their maximum crack openings were smaller than in the conventionally reinforced specimens with the same reinforcement ratio.

(4) The maximum crack opening is not necessarily adjacent to the maximum distance between cracks or located between two consecutive uncracked blocks of maximum total length. In this study, 11 of the considered 18 cracked schemes characteristic for the stabilized cracking stage (i.e. 61% of the cases) are in accordance with the conventional assumption of direct relation between the maximum crack width and maximum crack distance. In general, related to the defects in concrete structure and/or local damages of the bond with reinforcement, the maximum crack localization problem requires elaborate stochastic modelling algorithms.

(5) For the limited number of beams presented in this study, the ratio between the maximum and mean crack distances varied between 1.3 and 2.0, on average being 1.5, a number that is consistent with results by other researchers. It has been also found that this ratio is related to the reinforcement ratio, on average being 1.7 and 1.4, respectively, for the cases of p = 0.6% and 1.0%.

(6) The ratio of maximum and mean crack widths varied between 1.3 and 2.4 (1.7 on average) with lower values characteristic of members with larger total perimeter of the bars of the tensile reinforcement.

Acknowledgement

The authors gratefully acknowledge the financial support provided by the Research Council of Lithuania (Research Project MIP–050/2014).

References

[1] Foley C, Buckhouse E. Method to increase capacity and stiffness of reinforced concrete beams. ASCE Pract Periodical Struct Des Constr 1999;4(1):36–42.
[2] Ghali A, Favre R, Elbadry M. Concrete structures: stresses and deformations: analysis and design for serviceability. New York: CRC Press; 2006.
[3] Rostásy F, Koch R, Leonhardt F. Zur Mindestbewehrung für Zwang von Außenwänden aus Stahlleichtbeton. Deutscher Ausschuß für Stahlbeton 1976;267:1–107 [in German].
[4] Purainer R. Last- und Verformungsverhalten von Stahlbetonflächentragwerken unter zweiaxialer Zugbeanspruchung PhD Thesis. Munich, Germany: University of the Federal Armed Forces; 2005 [in German].
[5] Broms BB, Lutz LA. Effects of arrangement of reinforcement on crack width and spacing of reinforced concrete members. ACI J Proc 1965;62(11):1395–410.
[6] Nejadi S. Time-dependent cracking and crack control in reinforced concrete structures PhD Thesis. The University of New South Wales; 2005.
[7] Mias C, Torres L, Guadagnini M, Turon A. Short and long-term cracking behavior of GFRP reinforced concrete beams. Compos Part B: Eng 2015;77:223–31.
[8] Gribniak V, Cervenka V, Kaklauskas G. Deflection prediction of reinforced concrete beams by design codes and computer simulation. Eng Struct 2013;56:2175–86.
[9] Ley Urzáiz J, Calavera Ruiz J. Experimental study on the influence of cover a quantity of reinforcement with different diameters in the moment curvature relationship. Hormigón y Acero 2004;233(3):55–63 [in Spanish].
[10] Jakubovskis R, Kaklauskas G, Gribniak V, Weber A, Juknys M. Serviceability analysis of concrete beams with different arrangement of GFRP bars in the tensile zone. ASCE J Compos Constr 2014;18(5). 04014005-1-10.
[11] Ibars EO, del Arco DC, Marí Bernat AR. Interface behavior in fiber-reinforced polymer-strengthened beams subjected to transverse loads: maximum transferred force. ASCE J Compos Constr 2009;13(1):35–44.
[12] Si-Larbi A, Ferrier E, Hamelin P. Flexural behaviour of MRBC beams (multi-reinforcing bars concrete beams), promoting the use of FRHPC. Compos Struct 2006;74:163–74.
[13] Balazs GL, Bisch P, Borosnyoi A, et al. Design for SLS according to fib Model Code 2010. Struct Concr 2013;14(2):99–123.
[14] Balazs GL, Borosnyoi A. Cracking in CFRP prestressed members. In: Proc of the fifth international conference on fibre-reinforced plastics for reinforced concrete structures (FRPRCS-5). London: Thomas Telford; 2001. p. 609.
[15] Castel A, Vidal T, Francois R. Effective tension active cross-section of reinforced concrete beams after cracking. Mater Struct 2006;39:115–26.
[16] Barris C, Torres L, Comas J, Mias C. Cracking and deflections in GFRP RC beams: an experimental study. Compos Part B: Eng 2013;55:580–90.
[17] International Federation for Structural Concrete, fib. Model Code for Concrete Structures 2010. Berlin: Wilhelm Ernst & Sohn; 2013.
[18] Gribniak V, Kaklauskas G, Bacinskas D, Sung W-P, Sokolov A, Ulbinas D. Investigation of shrinkage of concrete mixtures used for bridge construction in Lithuania. Baltic J Road Bridge Eng 2011;6(2):77–83.
[19] Gribniak V, Kaklauskas G, Bacinskas D. Experimental investigation of shrinkage influence on tension stiffening of RC beams. Proc of the eighth international conference: creep, shrinkage and durability of concrete and concrete structures (ConCreep 8), vol. 1. London: CRC Press/Balkema; 2009. p. 571–7.
[20] Gribniak V, Kaklauskas G, Torres L, Daniunas A, Timinskas E, Gudonis E. Comparative analysis of deformations and tension-stiffening in concrete beams reinforced with GFRP or steel bars and fibers. Compos Part B: Eng 2013;50:158–70.
[21] Stramandinoli RS, La Rovere HL. An efficient tension-stiffening model for nonlinear analysis of reinforced concrete members. Eng Struct 2008;30(7):2069–80.
[22] Pérez Caldentey A, Corres Peiretti H. Medida experimental de las deformaciones a largo plazo de dos vigas hiperestáticas postesas. Hormigón y Acero 1999;211(1):2–29 [in Spanish].
[23] Rizkalla SH, Hwang LS. Crack prediction for members in uniaxial tension. ACI J Proc 1984;81(6):572–9.
[24] Williams A. Test on large reinforced concrete elements subjected to direct tension, Technical Report 562. Wexham Springs: Cement and Concrete Association; 1986.
[25] Calderón E, Fernández J. Investigación experimental sobre los modelos normativos de fisuración en piezas de hormigón armado sometidas a flexión pura. Informes de la Construcción 2010;62(518):43–56 [in Spanish].
[26] Gribniak V, Mang HA, Kupliauskas R, Kaklauskas G, Juozapaitis A. Stochastic tension-stiffening approach for the solution of serviceability problems in reinforced concrete: exploration of predictive capacity. Comput-Aided Civ Infrastruct Eng 2016;31(6):416–31. http://dx.doi.org/10.1111/mice.12183.
[27] Debernardi PG, Guiglia M, Taliano M. Shear strain in B-regions of beams in service. Eng Struct 2011;33(2):368–79.
[28] Borosnyói A, Snóbli I. Crack width variation within the concrete cover of reinforced concrete members. Építõanyag 2010;62(3):70–4.
[29] Debernardi PG, Guiglia M, Taliano M. Effect of secondary cracks for cracking analysis of reinforced concrete tie. ACI Mater J 2013;110(2):207–14.
[30] Debernardi PG, Taliano M. An improvement of the Eurocode 2 and fib Model Code 2010 methods for the calculation of crack width in r.c. structures. Struct Concr. http://dx.doi.org/10.1002/suco.201500033.
[31] Gudonis E, Kacianauskas R, Gribniak V, Weber A, Jakubovskis R, Kaklauskas G. Mechanical properties of the bond between GFRP reinforcing bars and concrete. Mech Compos Mater 2014;50(4):457–66.